

# Serendipitous Detections of XTE J1906+09 with the *Rossi X-ray Timing Explorer*

Colleen A. Wilson<sup>1</sup>, Mark H. Finger<sup>2</sup>, Ersin Göğüş<sup>3</sup>, Peter M. Woods<sup>2</sup>, Chryssa Kouveliotou<sup>1,2</sup>

*SD 50 Space Science Research Center, National Space Science and Technology Center, 320 Sparkman Drive, Huntsville, AL 35805*

[colleen.wilson-hodge@msfc.nasa.gov](mailto:colleen.wilson-hodge@msfc.nasa.gov)

## ABSTRACT

In 1996 during *Rossi X-ray Timing Explorer (RXTE)* observations of SGR 1900+14, the 89-s X-ray pulsar XTE J1906+09 was discovered. As a result of monitoring campaigns of SGR 1900+14, XTE J1906+09 was also monitored regularly in 1996 September, 1998 May-June, 1998 August-1999 July, and 2000 March-2001 January. A search for pulsations in these observations resulted in detections of only the two previously reported outbursts in 1996 September and 1998 August- September. Pulsed flux upper limits for the remaining observations indicate that XTE J1906+09 is a transient X-ray pulsar and therefore likely has a Be star companion. XTE J1906+09 was not detected with the *RXTE* All Sky Monitor. Pulse timing analysis of the second outburst revealed a sinusoidal signature in the pulse frequencies that is likely produced by periastron passage in an orbit. Fits to pulse phases using an orbital model and quadratic phase model have  $\chi^2$  minima at orbital periods of 26-30 days for fixed mass functions of 5, 10, 15, and  $20 M_\odot$ . The pulse shape showed intensity and energy dependent variations. Pulse phase spectroscopy was used to quantify the energy dependent variations. The phase averaged spectrum, using the pulse minimum spectrum as the background spectrum to eliminate effects from SGR 1900+14 and the galactic ridge, was well fitted by an absorbed power law with a high energy cutoff with column density  $N_H = (6 \pm 1) \times 10^{22} \text{ cm}^{-2}$ , photon index =  $1.01 \pm 0.08$ , cutoff energy  $E_{\text{cut}} = 11 \pm 1 \text{ keV}$ , and folding energy  $E_{\text{fold}} = 19 \pm 4 \text{ keV}$ . Estimated 2-10 keV peak fluxes, corrected for contributions from the galactic ridge and SGR 1900+14, are  $6 \times 10^{-12} \text{ ergs cm}^{-2} \text{ s}^{-1}$  and  $1.1 \times 10^{-10} \text{ ergs cm}^{-2} \text{ s}^{-1}$  for the 1996 and 1998 outbursts, respectively. XTE J1906+09 may be a member of an unusual class of Be/X-ray binaries that do not lie on the general spin period versus orbital period correlation with the majority of Be/X-ray binaries.

*Subject headings:* accretion—stars:pulsars:individual:(XTE J1906+09)—X-rays: binaries

## 1. Introduction

XTE J1906+09 is an 89-s accreting X-ray pulsar that was serendipitously discovered in a 1996 *Rossi X-ray Timing Explorer (RXTE)* Proportional Counter Array (PCA) observation of SGR 1900+14 (Marsden et al. 1998). Two outbursts

from XTE J1906+09 have been reported to date, in 1996 September (Marsden et al. 1998) and 1998 August-September (Takeshima & Corbet 1998). The 1996 energy spectrum was well fitted with either a thermal Bremsstrahlung spectral shape with temperature  $19.5 \pm 4.6 \text{ keV}$  and  $N_H = (7.7 \pm 5.2) \times 10^{22} \text{ cm}^{-2}$  or a power law with a photon index  $1.9 \pm 0.1$  and  $N_H = (10.8 \pm 4.0) \times 10^{22} \text{ cm}^{-2}$  (Marsden et al. 1998), when a fixed spectrum was assumed for the galactic ridge emission

<sup>1</sup>NASA's Marshall Space Flight Center

<sup>2</sup>Universities Space Research Association

<sup>3</sup>University of Alabama in Huntsville

(Valinia & Marshall 1998). The high absorption column density suggested that this source is at a distance of  $\gtrsim 10$  kpc. Marsden et al. (1998) suggest that XTE J1906+09 could have either a Be star companion or a supergiant companion that is under-filling its Roche lobe.

To date, about 80 accretion powered pulsars are known. These systems are often divided into 2 classes based on the mass of their companion: (1) high mass X-ray binaries (HMXBs) with OB companions (75 of the known systems) and (2) low mass X-ray binaries (5 of the known systems) with type A (or later) companions. The HMXBs are usually further divided into 3 classes based on the accretion mode of the system: (1) pulsars accreting from Roche lobe filling supergiants that tend to have short spin and orbital periods, (2) pulsars accreting from the strong stellar wind of a supergiant companion which is under-filling its Roche lobe that tend to have longer orbital periods and spin periods and show persistent but highly variable emission, and (3) pulsars accreting from the circumstellar disk around a Be star that as a population show a correlation between their spin and orbital periods (Corbet 1986; Waters & van Kerkwijk 1989).

Be/X-ray binaries are the most common HMXBs. They consist of a pulsar and a Be (or Oe) star, a main sequence star of spectral type B (or O) that shows Balmer emission lines (See e.g., Slettebak 1988 for a review.) The line emission is believed to be associated with circumstellar material shed by the Be star into its equatorial plane. The exact nature of the mass loss process is unknown, but it is thought to be related to the rapid rotation of the Be star, typically near 70% of the critical break-up velocity (Porter 1996). The equatorial material forms a slow, dense outflow, which is generally believed to fuel the X-ray outbursts. Near the Be star, the equatorial outflow probably forms a quasi-Keplerian disk (Quirrenbach et al. 1997; Hanuschik 1996). X-ray outbursts are produced when the pulsar interacts with the Be star's disk. Be/X-ray binaries typically show two types of outburst behavior: (i) giant outbursts, characterized by high luminosities and high spin-up rates (i.e., a significant increase in pulse frequency) and (ii) normal outbursts, characterized by lower luminosities, low spin-up rates (if any), and repeated occurrence at the orbital period (Stella, White, &

Rosner 1986; Bildsten et al. 1997).

The target of the *RXTE* observations, SGR 1900+14, is a member of a small class (4 objects), called Soft Gamma Repeaters (SGR), which exhibit brief ( $\sim 0.1$  s), intense ( $10^3$ – $10^4 L_{\text{Edd}}$ ) bursts of low energy gamma rays with recurrence times ranging from seconds to years (See Hurley 2000 for a recent review.) These objects also emit X-rays in quiescence. A spin period of 5.16-s was discovered in the quiescent emission of SGR 1900+14 (Hurley et al. 1999). The soft X-ray spectrum (0.1-10 keV) of SGR 1900+14 consists of a black-body ( $kT \sim 0.5$  keV) plus a power law component ( $\Gamma \sim -2$ ). The nominal unabsorbed 2-10 keV flux level is  $\sim 10^{-11}$  ergs  $\text{cm}^{-2} \text{ s}^{-1}$ . However, both the flux and spectrum of SGR 1900+14 have been shown to vary substantially during periods of burst activity (Woods et al. 2001). Effects from SGR 1900+14 were removed from the data whenever possible, but since SGR 1900+14 is always present in the field of view when XTE J1906+09 is active, it contaminates measurements of the total flux and average spectrum of XTE J1906+09.

In this paper we will present results of a search for additional outbursts of XTE J1906+09 in *RXTE* PCA observations from 1996-2001, detailed timing and spectral analysis of the 1998 outburst, a comparison of the 1998 and 1996 outbursts, and a discussion of the possible nature of this system.

## 2. Observations

The results presented in this paper involve data from the Proportional-Counter Array (PCA, Jahoda et al. 1996) and the High-Energy X-ray Timing Experiment (HEXTE, Rothschild et al. 1998) on the *Rossi X-ray Timing Experiment* (*RXTE*, Bradt, Rothschild, & Swank 1993). XTE J1906+09 is too weak to be detected with the *RXTE* All-Sky Monitor (ASM, Levine et al. 1996). The PCA consists of five identical xenon/methane multi-anode proportional counter units (PCU) sensitive to photons from 2-60 keV and has a total collecting area of  $6500 \text{ cm}^2$ . All 5 of the PCU are not always on, so in this paper, we have scaled all of our count rates to the rate that would have been observed in 5 PCU. Both the PCA and HEXTE are collimated instruments with an approximately circular field-of-view with a FWHM of about  $1^\circ$  (Jahoda et al. 1996; Rothschild et al.

1998). HEXTE consists of two clusters each containing four NaI/CsI scintillation detectors sensitive to photons in the 15-250 keV range. Each cluster has a collecting area of  $800 \text{ cm}^{-2}$ . One of the four detectors in cluster B has lost all energy resolution, so this detector is not included in our analysis. Each cluster can rock along mutually orthogonal directions to provide background measurements 1.5 to  $3.0^\circ$  away from the measured source every 16-128 s (Rothschild et al. 1998).

Because XTE J1906+09 is located  $33'$  from SGR 1900+14, a large number of PCA and HEXTE observations have been made of this region. Table 1 lists the *RXTE* Cycle, proposal identification number, number of observations, total on source time in kiloseconds, and the date ranges of the observations. Table 2 lists the percentage of time 5, 4, 3, or 2 PCUs were active for each row in Table 1.

### 3. Timing Analysis

#### 3.1. Frequency Search

Data from each observation were analyzed using FTOOLS<sup>4</sup> 5.0 (Blackburn 1995). An *RXTE* filter file was made for each observation. Good time intervals were selected where XTE J1906+09 was in the *RXTE* field-of-view, was not Earth occulted, and the time since the last SAA passage was greater than 30 s. Light curves with 16-s time resolution were produced selecting 2-30 keV Standard2 data from the top layer only of the PCA to improve signal to noise. Corresponding background light curves were produced using the FTOOL *pcabackest* with the faint source models. Net light curves were then produced by subtracting the background light curves from the Standard2 light curves. Variances on the net count rates were computed as  $\sigma_{\text{net}}^2 = \sigma_{\text{total}}^2 + (0.01R_{\text{back}})^2$  where  $R_{\text{back}}$  is the model background rate. The background model has an estimated systematic error of 1% (Jahoda et al. 1996). Because these observations are optimized for SGR 1900+14, not XTE J1906+09, the PCA pointing direction was frequently offset significantly from the XTE J1906+09 position. Pointing offsets to XTE J1906+09 (filled triangles) and the bright 440-s pulsar 4U 1907+09 (open squares) are shown

<sup>4</sup><http://heasarc.gsfc.nasa.gov/ftools>

in Figure 1. Error bars denote the standard deviation in the pointing offset. Scanning observations have the largest error bars. Gaps indicate times when the PCA did not observe this region of the sky. The FTOOL *xtecol* was used to create collimator corrected light curves for the offset pointing. These light curves were then barycentered to the solar system barycenter using the FTOOLS *fbary* (before 2000 December 31) and *faxbary* (after 2000 December 31). Bursts from SGR 1900+14, present in observations from 1998 August-September, were removed from the data using a simple algorithm that discarded data outliers. Outliers were defined as points where  $|R - R_{\text{med}}| > R_{\text{med}}$  where  $R$  is the background subtracted count rate (in 16-s intervals) and  $R_{\text{med}}$  is the median background subtracted count rate (in 16-s intervals) for that observation.

A search for pulsations from XTE J1906+09 was performed for each observation. Observations separated by less than 4 *RXTE* orbits were combined and count rates for all observations were corrected for varying numbers of PCUs. The data from each observation were fitted with a model consisting of a constant term plus a second order Fourier expansion in a pulse phase model. The pulse phase model used was of the form  $\phi = \nu(t - t_{\text{mid}})$  where  $\nu$  is a trial frequency,  $t$  is the barycentered time associated with the net count rate, and  $t_{\text{mid}}$  is the midpoint time of the observation. The trial frequency search grid consisted of 81 evenly spaced frequencies from 11.168 to 11.261 mHz. To correct the variances on the harmonic<sup>5</sup> amplitudes in the Fourier expansion for aperiodic noise in the power spectrum (due either to XTE J1906+09 or other sources in the *RXTE* field of view), we first computed the average Leahy normalized (Leahy et al. 1983) power spectrum for 1 ksec segments of data and subtracted the pulsed component. Then we computed the average power  $\bar{P}_n$  for the frequency intervals  $[n\nu_0/2, 3n\nu_0/2]$ , where  $\nu_0$  is the pulse frequency and  $n = 1, 2, \dots$  is the harmonic number. If  $\bar{P}_n$  was greater than the expected Poisson level of 2.0, we multiplied the variances on the corresponding harmonic amplitudes by  $\bar{P}_n/2$  to correct for aperiodic noise. This correction accounts for aperiodic

<sup>5</sup>In this paper, harmonics are defined as  $n\nu$  where  $n = 1, 2, 3, \dots$  and  $\nu$  is the pulse frequency.

noise dependent systematic differences in sensitivity from observation to observation. The best fit frequency for each observation was determined using a modified  $Z_2^2$  statistic (Buccheri et al. 1983), which we will call  $Y_n$ , that incorporates the corrected variances (Finger et al. 1999). For the best fit frequency, the root-mean-squared (rms) pulsed amplitude was also computed. Results of the XTE J1906+09 frequency search are shown in Figure 2. Monte Carlo simulations were run to determine detection confidence levels. From  $10^5$  trials using the time structure of the observation on 1999 January 9 (a typical observation lasting about 15 ksecs with 10 ksecs on source) we determined detection confidence levels of 99% ( $Y_2 \gtrsim 14.6$ ), 99.9% ( $Y_2 \gtrsim 20.9$ ), and 99.99% ( $Y_2 \gtrsim 29.0$ ). These confidence intervals do not take into account effects from 4U 1907+09.

The bright 440-s X-ray pulsar 4U 1907+09 (in't Zand, Baykal, & Strohmayer 1998) is located near both XTE J1906+09 and SGR 1900+14 and was present in the PCA field of view for some of the observations. Before performing a search for pulsations from 4U 1907+09, the net 2-30 keV light curves were corrected for the PCA collimator response to the offset pointing to 4U 1907+09 and were barycentered for its position. To test whether or not this source was active, we performed a coarse frequency search over a grid of 31 evenly spaced frequencies from 2.225 to 2.341 mHz using the observations where 4U 1907+09 was in the PCA field of view. By chance, the fifth harmonic of 4U 1907+09's 440-s period is about 88-s, quite close to the 89-s period of XTE J1906+09, so only the first 4 harmonics of 4U 1907+09 were used in the frequency search. The two sources can usually be easily separated in power spectra and were successfully separated in all observations used for subsequent pulse phase analysis. The frequency search for 4U 1907+09 told us when that source was active and when we needed to check for contamination in XTE J1906+09 measurements. Results of the 4U 1907+09 frequency search are shown in Figure 3. From  $10^5$  Monte Carlo trials using the time structure of the observation on 1999 January 5 (a typical observation lasting about 15 ksecs with 10 ksecs of on source time), we determined detection confidence levels of 99% ( $Y_4 \gtrsim 26.2$ ), 99.9% ( $Y_4 \gtrsim 39.3$ ), and 99.99% ( $Y_4 \gtrsim 47.3$ ).

### 3.2. Pulse Phase Analysis

To generate pulse phase measurements, we first made 2-30 keV light curves with 1-s time resolution for 15 PCA observations (MJD 50337-50346, 1996 September 11-20 in science data mode E\_125us\_64M\_0\_1s) during the first outburst and 28 PCA observations (MJD 51056-51086, 1998 August 31-September 30, 13 in science data mode E\_125us\_64M\_0\_1s, 15 in science data mode Good Xenon) during the second outburst. The observations used for pulse phase analysis included all those with significant frequency detections in our grid search plus a few observations either side of those intervals of frequency detections. The data were background subtracted using a spline fit to the 16-s background model count rates generated with the FTOOL *pcabackest* and errors on the net count rates were computed assuming a 1% systematic error on the background. Collimator corrections generated for Standard 2 data using the FTOOL *xtecol* were applied manually. For each observation within each outburst, initial pulse profiles were created by fitting harmonic amplitudes in a Fourier series expansion in a phase model of the form

$$\phi = \bar{\nu}(t - t_{\text{mid}}) \quad (1)$$

where  $\bar{\nu}$  is the average pulse frequency for each outburst (11.2150 mHz and 11.2158 mHz for the first and second outbursts, respectively) from detections in our grid search and  $t_{\text{mid}}$  is the mid-time of each outburst. Template pulse profiles were also created by fitting harmonic amplitudes in a Fourier expansion in a phase model of the form in Equation 1. For the first outburst, we used the brightest interval 50343.533-50343.838 (1996 September 17) to generate the template profile, with a pulse frequency of 11.216 mHz from our grid search. For the second outburst, we used a moderate intensity interval MJD 51072.829-51072.989 (1998 September 16) to create the template, with a pulse frequency of 11.213 mHz from our grid search results. Figure 4 (top panel) shows the pulse profile used to generate the template for the first outburst. Only the first 6 harmonics were significant. The bottom panel shows the pulse profile used to create the template for the second outburst. Only the first 12 harmonics were significant. The mean has been subtracted from these pulse profiles and for all other pulse pro-

files in this paper because the mean count rate includes contributions from XTE J1906+09, SGR 1900+14, and in some observations, 4U 1907+097. Since RXTE is not an imaging instrument, the relative contribution from each of the three sources cannot be determined. Template pulse profiles were normalized so that the sum of the squares of the harmonic amplitudes was equal to 2. Phase offsets and pulsed intensities were calculated by cross-correlating the fitted profile for each observation with the template profile. In the cross-correlations, 6 harmonics were used for the first outburst and 12 harmonics for the second outburst. Using the measured pulse frequencies from our frequency search, we determined that we could phase connect data from only 8 observations in the first outburst (MJD 50340.9-50344.8, 1996 September 14-19) and 23 observations from the second outburst (MJD 51056.44- 51075.64, 1998 August 31-September 20). We fitted the connected phase measurements from each outburst with a polynomial model of the form

$$\phi = \sum_{i=0}^n c_i (t - t_0)^i \quad (2)$$

where  $c_i$  are coefficients given in Table 3 and  $t_0$  is an epoch. Residuals to these polynomial models are shown in Figure 5. Pulse frequencies computed by differencing adjacent connected phases show a period of spin-up followed by spin-down followed by spin-up, shown in Figure 6 (top panel). This is strongly suggestive of an orbital signature and is consistent with either a short, nearly circular orbit or with periastron passage in a much longer eccentric orbit. No clear signature is seen in measurements from the first outburst; however, this is not surprising since the phase connected measurements only span 4 days and the outburst was much weaker.

To investigate possible orbits, we fitted a quadratic phase model and an orbit with a fixed period and fixed mass function to 23 connected phase measurements from the second outburst. The connected phase measurements from the first outburst spanned too short a time to improve our fits. A grid of 300 orbital periods from 20 to 320 days was searched for fixed mass functions of  $f(M) = 5, 10, 15, 20 M_\odot$ . (Be stars typically have masses in the range  $8-20 M_\odot$ .) Figure 7 shows  $\chi^2$  versus orbital period for the selected mass func-

tions. For all four mass functions, the best fit period was in the range 26-30 days, the eccentricity was low, 0.03-0.06, and the frequency derivative was relatively large  $1 - 2 \times 10^{-11} \text{ Hz s}^{-1}$ . The periastron epoch was in the range JD2451055-57 and the periapse angle was in the range 126-144°. We advise caution using these parameters because this apparent orbital signature was observed in a single 25-day interval. Observations of additional outbursts are needed to confirm these parameters.

### 3.3. Pulse Profiles

The 2-30 keV pulse profiles shown in Figure 4 are similar despite being from very different time intervals and intensities. Both consist of 2 main peaks with the first peak (phase  $\sim 0.1 - 0.4$  top panel) being narrower than the second peak (phase  $\sim 0.5 - 1.1$  top panel). During the 1996 September outburst, the source was much fainter than during the 1998 outburst. Comparing the two profiles suggests that a correlation between the pulse shape and intensity may be present. The first main peak is much brighter relative to the second main peak in the pulse profile from the stronger outburst than in the weaker outburst. To further investigate this effect, we phase aligned data from the 1998 outburst using the phase model in Table 3. The phase aligned harmonic amplitudes were averaged over 5 bands of 2-30 keV rms pulsed flux: 0-5, 5-10, 10-15, 15-20, and 20-25 counts  $\text{sec}^{-1}$ . Figure 8 shows the average profiles from the 5 intensity bands (top 5 panels) and the profile from the brightest interval in the 1996 outburst (bottom panel and top panel of Figure 4). The intensity of the first main peak (phase  $\sim 0.2 - 0.5$ ) increases dramatically as the pulsed flux increases. The second main peak (phase  $\sim 0.6 - 1.2$ ) gradually evolves from a broad peak approximately equal in intensity to the first main peak to multiple peaks with considerable structure as the pulsed flux increases. Within the 1998 outburst, the pulse shape appears to be correlated with intensity. The pulse profile from the 1996 outburst looks consistent with the low intensity profiles from the 1998 outburst, suggesting that the pulse shape-intensity correlation holds for both outbursts.

Next we extracted light curves in several energy bands to look for energy dependence in the shape of the pulse profile. These light curves were background subtracted, collimator corrected, and

barycentered. For the first outburst, the 5 brightest observations when 4U 1907+09 was not present in the PCA field of view (MJD 50343.6-50344.8, 1996 September 17-18) were combined and epoch-folded in the time domain using the phase model in Table 3 in 3 energy bands shown in Figure 9. Corresponding background subtracted event mode HEXTE light curves were extracted using the FTOOL *hxltcurv*, barycentered, and collimator corrected. Marsden et al. (1998) report a detection of XTE J1906+09 with HEXTE during this outburst, however our HEXTE pulse profiles are consistent with a constant value, i.e., non-detection of XTE J1906+09. We are not certain which observations Marsden et al. (1998) used, since there were no *RXTE* observations of this region on 1996 August 16-19, the dates reported in their paper. It appears that they also used the 1996 September observations based on our comparisons with their PCA results. Figure 2 in Marsden et al. (1998) shows folded pulse profiles from HEXTE plotted in units of counts  $\text{bin}^{-1}$ . If we fold our HEXTE data, also uncorrected for the total time in each bin, we see a similar profile. When we correct for the total time in each phase bin (i.e., plotting in units of counts  $\text{s}^{-1}$ ), our profiles are consistent with a constant value. Further, the 20-30 keV HEXTE profile in Marsden et al. (1998) does not appear to agree with the PCA profile in the same band, while in the 1998 outburst, where we clearly detect XTE J1906+09 with HEXTE and the PCA, the profiles in this band agree well.

For the second outburst, we selected the observation made on MJD 51064 (1998 September 8) because it was near the peak of the outburst, it was a long observation ( $\sim 8300$  s of on-source time), and 4U 1907+09 was not present in the PCA field of view. PCA light curves were extracted in 5 energy bands, 2-5, 5-10, 10-15, 15-20, and 20-30 keV. HEXTE light curves were extracted in 3 energy bands 15-20 keV, 20-30 keV, and 30-100 keV. HEXTE was in “staring” mode for this observation, so no background measurements were available. These light curves were epoch-folded using the phase model in Table 3 and are shown in Figure 10. The collimator correction was applied to the HEXTE pulse profiles by multiplying the epoch-folded mean-subtracted rates by the correction factor computed using the FTOOL *xtecol*. At low energies ( $< 10$  keV), the

pulse profile consists of 3 peaks: a bright peak from phase  $\sim 0.21 - 0.50$ , a broad peak from phase  $\sim 0.6 - 1.05$ , and a narrow peak from phase  $\sim 1.07 - 1.15$ . As energy increases, the brightest peak remains distinct, the minimum following the first peak becomes broader, and the second two peaks blend into a broad shoulder.

#### 4. Spectral Analysis

We selected the  $\sim 8300$  s observation on MJD 51064 (1998 September 8) for extraction of a phase averaged spectrum of XTE J1906+09. This observation was selected because no bursts from SGR 1900+14 were present and 4U 1907+09 was not in the *RXTE* field-of-view. As mentioned above, HEXTE was in staring mode for this observation, so HEXTE spectra were not used because background data were not available. PCA data had better signal to noise for the 15-30 keV band, where XTE J1906+09 was detected, than HEXTE. Spectra were extracted from Good Xenon (256 channel, photon time tagged) PCA data for the top Xenon layer only and corresponding PCA background spectra were generated using the faint source background model in *pcabackest*. Response matrices were created using the FTOOL *pcarsp* with the XTE J1906+09 location. The phase averaged PCA data were fitted using XSPEC 11.0.1. For the spectral fits, PCA data in the energy range 2.5-30 keV were used. The spectrum was best fitted with a typical accreting X-ray pulsar spectrum, an absorbed power law with a high energy cutoff + a Gaussian iron line. The best fit parameters are listed in the second column of Table 4. Evidence for an iron line at  $\sim 6.6$  keV is suggested by our spectral fits. The 2-10 keV flux computed using this spectral model is  $1.59 \times 10^{-10}$   $\text{ergs cm}^{-2} \text{ s}^{-1}$ . From Figure 2 in Woods et al. (2001), we estimated the 2-10 keV flux from SGR 1900+14 as  $3.2 \times 10^{-11}$   $\text{ergs cm}^{-2} \text{ s}^{-1}$ . The spectral fit from the 1996 outburst in Marsden et al. (1998), gave a 2-10 keV flux of  $1.67 \times 10^{-11}$   $\text{ergs cm}^{-2} \text{ s}^{-1}$  for the galactic ridge. Subtracting the contaminating fluxes, we estimated the 2-10 keV flux from XTE J1906+09 was  $1.1 \times 10^{-10}$   $\text{erg cm}^{-2} \text{ s}^{-1}$ . This flux is listed in Table 4. Observations with an imaging instrument are needed to fully separate the un-pulsed component of the XTE J1906+09 spectrum from the galactic ridge and SGR 1900+14.

To investigate if the iron line was likely due to XTE J1906+09 and to look for spectral evolution, we generated phase averaged spectra, background spectra, and response matrices as described in the previous paragraph for 10 observations from 1998 August 31 - September 9 (MJD 51056-51065) using Standard 2 (129 channel, 16-s time resolution) PCA data for the top Xenon layer only. Observations after 1998 September 9 were not used because 4U 1907+09 was in the PCA field of view. For each observation, PCA data in the energy range 2.5-30 keV were fitted with an absorbed power law with a high energy cutoff + a Gaussian iron line. As the intensity increased, the photon power law index decreased from  $\Gamma \sim 2$  to  $\Gamma \sim 1.2$ . This apparent spectral hardening may be intrinsic to the source or it could be due to contamination from the softer spectra of SGR 1900+14 ( $\Gamma \sim 2$ , Woods et al. 2001) and the galactic ridge ( $\Gamma \sim 1.8$ , Valinia & Marshall 1998). Figure 11 shows the integrated flux of the iron line versus the rms pulsed flux for each observation. The iron line flux appears to be correlated with the pulsed flux, with a correlation coefficient of 0.93 and a chance probability of  $10^{-4}$ ; however, the errors on the iron line flux are fairly large. This correlation suggests that the iron line is intrinsic to XTE J1906+09.

To study the energy spectrum of the pulsed emission we created phase resolved energy spectra for 20 equal phase intervals with the FTOOL *phase-bin* using PCA good xenon data from MJD 51064 (1998 September 8). Instead of using the background model to generate the background spectrum, we used the measured spectrum at pulse minimum (phase 0.5-0.6) as the background spectrum in XSPEC. These spectra were well fitted with a typical pulsar model, an absorbed power law with a high energy cutoff. No iron line was required to obtain acceptable fits. The phase averaged spectrum was again fitted, but this time using the pulse minimum as the background spectrum. The parameters of this fit are listed in the third column of Table 4.

Fit results for the spectra from each of the 19 phase intervals using the pulse minimum spectrum as the background are shown in Figure 12. The fit results from the phase averaged spectrum are plotted as dotted lines. Panel (a) shows the mean-subtracted 2-30 keV count rate in each phase bin. Arrows indicate the bin used as the background

spectrum. The absorption column density  $N_H$ , plotted in panel (b), increases for the bin centered on phase 0.15. This corresponds to the dip at phase  $\sim 0.15$  in Figure 10, just before the bright peak. This dip becomes shallower with increasing energy and has disappeared above about 15 keV. Panels (c), (d), and (e) show the power law photon index, the cutoff energy  $E_{\text{cut}}$ , and the e-folding energy  $E_{\text{fold}}$ , respectively. These panels show evidence for spectral softening around the pulse minimum in the phase range  $\sim 0.4 - 0.6$ . In Figure 10 the pulse minimum becomes broader with increasing energy, also indicating spectral softening. The hardest spectral index is at phase 0.15, corresponding to the dip present at low energies at phase  $\sim 0.15$ , that disappears as energy increases, suggesting spectral hardening.

Using our spectral model, we computed a phase averaged 2-10 keV pulsed flux of  $7.23 \times 10^{-11}$  ergs  $\text{cm}^{-2} \text{ s}^{-1}$ . Taking the ratio of the pulsed flux to the corrected 2-10 keV total flux in Table 4 gives a peak-to-peak pulse fraction of  $\sim 66\%$ . If we assume this pulse fraction is constant for both outbursts, we estimate the total 2-10 keV flux in the 1996 outburst was  $6 \times 10^{-12}$  ergs  $\text{cm}^{-2} \text{ s}^{-1}$  from our pulsed flux measurements. The quiescent 2-10 keV flux from SGR 1900+14 is believed to be constant at a level of about  $1 \times 10^{-11}$  ergs  $\text{cm}^{-2} \text{ s}^{-1}$  (Woods et al. 2001). Hence, the combined XTE J1906+09 and SGR 1900+14 would be  $1.6 \times 10^{-11}$  ergs  $\text{cm}^{-2} \text{ s}^{-1}$ , consistent with the 2-10 keV flux measured from both sources by Marsden et al. (1998). This suggests that the XTE J1906+09 pulse fraction in the 2-10 keV band is approximately constant at 66%.

## 5. Discussion

The sky region including XTE J1906+09 was regularly monitored with *RXTE* every few days from 1998 August to 1999 July and again from 2000 March - 2001 January as part of our guest investigation to observe SGR 1900+14. Prior to the monitoring campaign, this sky region was observed regularly for about 2 weeks in 1996 September and again in 1998 May-June. A search for pulsations from XTE J1906+09 in these observations resulted in the detection of two outbursts, 1996 September 17-18 (MJD 50343-50344) and 1998 August 30 - September 24 (MJD 51056-

51080). Both outbursts have been previously reported (Marsden et al. 1998; Takeshima & Corbet 1998). Unfortunately our data cannot unambiguously determine the orbital period of the system. The two detected outbursts are separated by about 730 days. This spacing may be an integer multiple of the orbital period, since normal outbursts in transient X-ray pulsars usually occur near periastron passage. Outbursts similar to the 1996 outburst, which was detected for only 2 days in the frequency grid search and for about 4 days in pulse phase measurements, could have been easily missed because the observations of the region were usually at least few days apart even during the regular monitoring. The non-detection of XTE J1906+09 in most of the observations tells us that this source is a transient source. The known companions of transient X-ray pulsars are all Be stars (with the exception of GRO J1744–28), hence XTE J1906+09 most likely has a Be star companion.

The two outbursts differ considerably in peak intensity and duration (Figure 2). The second outburst lasted about 25 days and was a factor of  $\sim 20$  brighter in 2-30 keV pulsed flux than the first one which was very short, 2-4 days. Although the second outburst was brighter and longer, it is unlikely that it is a giant outburst like that observed in some Be X-ray binaries because giant outbursts are typically near Eddington luminosity at their peaks (e.g. Bildsten et al. 1997). Assuming a distance of  $\lesssim 20$  kpc, the 2-30 keV peak luminosity of the second outburst is  $\lesssim 2 \times 10^{37}$  ergs  $\text{cm}^{-2}$   $\text{s}^{-1}$ , consistent with a normal outburst. In the pulse frequencies measured by differencing connected phase measurements, we see a distinct sinusoidal signature that is likely due to the orbit of XTE J1906+09 (Figure 6). Two possible scenarios could produce this signature: (1) a short ( $\sim 30$  day), nearly circular, orbit or (2) periastron passage in a long, eccentric, orbit. Accreting X-ray pulsar systems with short, nearly circular, orbits are typically persistent systems (Bildsten et al. 1997) and XTE J1906+09 is clearly a transient system. The second case of periastron passage in a long, eccentric, orbit is what one would expect from a Be/X-ray transient system. Fits of a quadratic phase model and an orbit with a fixed orbital period and mass function yielded  $\chi^2$  minima for orbital periods of 26-30 days and ec-

centricities of 0.03-0.06.

An orbital period of 26-30 days is shorter than what would be expected from the general correlation between orbital and pulse periods in Be/X-ray transients (Corbet 1986; Waters & van Kerkwijk 1989). 4U 0728–25 (Corbet & Peele 1997) and possibly GRO J2058+42 (Wilson, Finger, & Scott 2000; Wilson et al. 1998; Corbet, Peele, & Remillard 1997) may also have shorter orbital periods than expected. 4U 0728–25 is a confirmed Be/X-ray binary with a 103.2-s pulse period and a 34.5 day outburst period. GRO J2058+42 is a 195.6-s pulsar with either a 55 or 110 day orbital period. Odd-even pulsed flux variations in outbursts observed with BATSE may indicate the orbital period is 110 days (Wilson et al. 1998); however, observations with the *RXTE* ASM and PCA do not show clear evidence for differences between the outbursts, suggesting an orbital period of 55 days (Wilson, Finger, & Scott 2000; Corbet, Peele, & Remillard 1997). In both cases, the periods are outburst recurrence times, so pulse timing analysis of data with appropriate phase coverage is needed to confirm these as orbital periods. These three sources may be members of an unusual class of Be/X-ray binary that does not lie on the general spin-orbital period correlation (Corbet 1986; Waters & van Kerkwijk 1989) with most Be systems. Our grid searches also suggest that the eccentricity in XTE J1906+09 may be quite low. Four Be/X-ray binaries have measured orbits with low eccentricities, X Per ( $e = 0.11$ , Delgado-Marti et al. (2001)), XTE J1543–568 ( $e < 0.03$ , in't Zand, Corbet, & Marshall 2001), GS 0834–430 ( $0.1 \lesssim e \lesssim 0.17$ , Wilson et al. 1997), and 2S 1553–542 ( $e < 0.09$ , Kelley, Rappaport, & Ayasli 1983). The system that appears most similar to XTE J1906+09 is 2S 1553–542, which has a spin period of 9.3-s and an orbital period of 30.6 days. However, the orbit of this system was measured using a 20 day observation and the source has not been observed in outburst again. In both 2S 1553–542 and XTE J1906+09, the orbital parameters were determined using less than one orbital period and should be treated with caution. Strong intrinsic torques, often correlated with the intensity of the pulsar (Finger et al. 1999; Bildsten et al. 1997), could easily produce misleading results in a short stretch of data. Coupling between intrinsic torques and the orbit could lead to erroneous or-

bial parameters. Observations of additional outbursts from both sources are needed to confirm the orbital parameters.

If XTE J1906+09 is a low eccentricity system, it is surprising that it appears to show only isolated normal outbursts. At least one other system, Cep X-4 (Wilson, Finger, & Scott 1999) also showed isolated normal outbursts, but its orbit is unknown. The flux level of 2S 1553–542 was not reported by Kelley, Rappaport, & Ayasli (1983), so it is unclear whether it underwent a giant or normal outburst. The viscous decretion disk model, which accounts for most properties of Be stars, predicts the truncation of the circumstellar disk around the Be star, due to the presence of the neutron star. In systems with low eccentricities ( $e < 0.2$ ), this model predicts that the truncation mechanism would be so effective that no normal outbursts would be seen at all. Only giant outbursts would be expected when the disk was strongly disturbed (Okazaki & Negueruela 2001). However this model fails to explain the series of normal outbursts in GS 0834–430 (Wilson et al. 1997). It also does not easily explain the 103.2-s pulsar 4U 0728–26, which has not shown giant outbursts, but shows a 34.5 day modulation in its persistent flux (Corbet & Peele 1997). Perhaps a moderate perturbation in the Be disk, not large enough to produce a giant outburst, could produce the isolated normal outbursts we observe in XTE J1906+09.

The transient nature of XTE J1906+09 suggests that it is likely a member of a Be/X-ray binary system. *RXTE* PCA scans during the second outburst of XTE J1906+09 localized it to a 2' radius error circle centered on  $\alpha = 19^h 05^m 20^s$ ,  $\delta = 9^{\circ} 02'.5$ , J2000 (Takeshima & Murakami 1998). No objects were found in the error circle in the Simbad<sup>6</sup> database. We searched the catalogs at the High Energy Astrophysics Science Archive Research Center<sup>7</sup> for a possible counterpart. The ROSAT All-Sky Survey Faint Source catalog contained no sources within 30' of XTE J1906+09. Although pointed observations of SGR 1900+14 were made with EUVE and BeppoSAX, XTE J1906+09 was outside the field-of-view in all cases. The ASCA Galactic Plane Survey (Sugizaki et

al. 2001) did not detect an X-ray source brighter than  $10^{-12.5}$  ergs  $\text{cm}^{-2}$   $\text{s}^{-1}$  within 52' of XTE J1906+09. However, the 2' error circle contains no shortage of stars. In the USNO A-2 catalog<sup>8</sup>, we found 41 stars in the error circle, with B-magnitudes ranging from 15.9 to 20.0 and R-magnitudes ranging from 14.0 to 18.4. If this sample of stars ranges over all distances (as is likely in this case), each star will have its own color correction depending on distance, so comparing objects in the field is difficult. Our  $N_{\text{H}}$  values from Table 4 imply an extinction of  $Av \gtrsim 15$  (Predehl & Schmitt 1995), which makes it unlikely we will see the companion in the visible range. One infrared source was found in the error circle at  $\alpha = 19^h 05^m 15.38^s$ ,  $\delta = 09^{\circ} 03' 39.6''$ , J2000 in the MSX5C<sup>9</sup> Infrared Point Source Catalog (Egan et al. 1999); however, this object does not appear in the Catalog of Infrared Observations<sup>10</sup>. An X-ray observation with a very sensitive imaging instrument such as *Chandra* or *XMM*, since XTE J1906+09 would most likely be in quiescence, is needed to improve the location accuracy before a companion can be identified.

This research has made use of data obtained from the High Energy Astrophysics Science Archive Research Center (HEASARC), provided by NASA's Goddard Space Flight Center. This research has also made use of the SIMBAD database, operated at CDS, Strasbourg, France. We thank M.J. Coe for helpful discussions.

## REFERENCES

Bildsten, L. et al. 1997, *ApJS*, 113, 367  
 Blackburn, J.K. 1995, in *ASP Conf. Ser.*, Vol. 77, *Astronomical Data Analysis and Software Systems IV*, ed. R.A. Shaw, H.E. Payne, & J.J.E. Haynes (San Francisco:ASP), 367  
 Bradt, H.V., Rothschild, R.E., & Swank, J.H. 1993, *A&AS*, 97, 355  
 Buccheri, R. et al. 1983, *A&A*, 128, 245  
 Corbet, R.H.D. 1986, *MNRAS*, 220, 1047

<sup>6</sup><http://simbad.u-strasbg.fr>

<sup>7</sup><http://heasarc.gsfc.nasa.gov>

Corbet, R.H.D. & Peele, A.G. 1997, *ApJ*489, L83

Corbet, R.H.D., Peele, A.G., & Remillard, R. 1997, *IAU Circ.*, 6556

Delgado-Marti, H., Levine, A.M., Pfahl, E., & Rappaport, S. 2001, *ApJ*, 546, 455

Egan M.P. et al. 1999, The Midcourse Space Experiment Point Source Catalog, Version 1.2 (June 1999), Air Force Research Lab. Technical Rep. AFRL-VS-TR-1999-1522

Finger, M. H., Bildsten, L., Chakrabarty, D., Prince, T. A., Scott, D. M., Wilson, C. A., Wilson, R. B., & Zhang, S. N. 1999, *ApJ*, 517, 449

Hanuschik, R.W. 1996, *A&A*, 308, 170

Hurley, K. et al. 1999, *ApJ*, 510, L111

Hurley, K. 2000, in *AIP Conf. Proc.* 526, Gamma-Ray Bursts: Fifth Huntsville Symp., eds. R.M. Kippen, R.S. Mallozzi, & G.J. Fishman (New York:AIP), 763

in't Zand, J.J.M., Baykal, A. & Strohmayer, T.E. 1998, *ApJ*, 496, 386

in't Zand, J.J.M., Corbet, R.H.D., Marshall, F.E. 2001, *ApJ*, 553, 165

Jahoda, K. et al. 1996, EUV, X-ray, and Gamma-Ray Instrumentation for Astronomy VII, *SPIE Proc.* 2808, ed. O.H.V. Sigmund & M.Gumm (Bellingham:SPIE), 59

Kelley, R.L., Rappaport, S., & Ayasli, S. 1983, *ApJ*, 274, 765

Leahy, D.A. et al. 1983, *ApJ*, 266,160

Marsden, D., Gruber, D.E., Heindl, W.A., Pelling, M.R., Rothschild, R.E. 1998, *ApJ*, 502, L129

Okazaki, A.T. & Negueruela, I. 2001, *A&A*, in press, *astro-ph/0108037*

Porter, J.M. 1996, *MNRAS*, 280, L31

Predehl, P. & Schmitt, J.H.M.M 1995, *A&A*, 293, 889

Quirrenbach, A. et al. 1997, *ApJ*, 479, 477

Rothschild, R.E. et al. 1998, *ApJ*, 496, 538

Slettebak, A. 1988, *PASP*, 100, 770

Stella, L., White, N.E., & Rosner, R. 1986, *ApJ*, 308, 669

Sugizaki, M. et al. 2001, *ApJS*, 134, 77

Takeshima, T. & Corbet, R. H. D. 1998, *IAU Circ.* No. 7008

Takeshima, T. & Murakami, T. 1998, *IAU Circ.* No. 7032

Valinia, A. & Marshall, F.E. 1998, *ApJ*, 505, 134

Waters, L.B.F.M. & van Kerkwijk, M.H. 1989, *A&A*, 223, 196

Wilson, C.A. et al. 1997, *ApJ*, 479, 388

Wilson, C.A. et al. 1998, *ApJ*, 499, 820

Wilson, C.A., Finger, M.H., & Scott, D.M. 1999, *ApJ*, 511,367

Wilson, C.A., Finger, M.H., & Scott, D.M. 2000, in *AIP Conf. Proc.* 510, The Fifth Compton Symposium, eds. M.L. McConnell & J. Ryan (New York: AIP), 208

Woods, P.M. et al. 2001, *ApJ*, 552, 748

TABLE 1  
*RXTE PCA OBSERVATIONS WITH XTE J1906+09 IN THE PCA FIELD OF VIEW*

Cycle	Proposal ID	No. Obs.	On-Source Time (ksec)	Dates	MJD
AO1	10228	19	97.7	1996 Sep 4-1996 Sep 20	50330-50346
AO3	30197	12	46.1	1998 May 31-1998 Aug 29	50964-51054
AO3	30410	50	178.6	1998 May 29-1998 Dec 22	50962-51169
AO4	40130	38	266.6	1999 Jan 3-1999 Jul 28	51181-51387
AO4	40130	9	51.4	2000 Mar 10-2000 Mar 23	51613-51626
AO5	50142	50	189.9	2000 Mar 29-2000 Aug 13	51632-51769
AO5	50421	61	259.4	2000 Sep 4-2001 Jan 6	51791-51915

NOTE.—Observation start and stop times can be obtained from the web-site <http://heasarc.gsfc.nasa.gov>

TABLE 2  
PERCENTAGE OF TIME PCUS WERE ACTIVE

Proposal ID	5 PCUs on	4 PCUs on	3 PCUs on	2 PCUs on
10228	58%	27%	15%	0%
30197	8%	87%	5%	0%
30410	58%	35%	6%	0%
40130 <sup>a</sup>	48%	39%	13%	0%
40130 <sup>b</sup>	0%	10%	90%	0%
50142	2%	43%	52%	3%
50421	16%	43%	39.5%	1.5%

<sup>a</sup>1999 observations

<sup>b</sup>2000 observations

TABLE 3  
POLYNOMIAL FITS TO PULSE PHASE MEASUREMENTS

Coefficient	Outburst 1	Outburst 2
$c_0$ (cycles)	$0.048 \pm 0.006$	$-0.2938 \pm 0.0009$
$c_1$ (cycles day $^{-1}$ )	$969.008 \pm 0.008$	$968.6979 \pm 0.0002$
$c_2$ (cycles day $^{-2}$ )	$(-6 \pm 1) \times 10^{-2}$	$(-1.492 \pm 0.008) \times 10^{-2}$
$c_3$ (cycles day $^{-3}$ )	$(-1.3 \pm 0.4) \times 10^{-3}$	$(2.269 \pm 0.008) \times 10^{-3}$
$c_4$ (cycles day $^{-4}$ )	...	$(1.30 \pm 0.02) \times 10^{-4}$
$c_5$ (cycles day $^{-5}$ )	...	$(-2.8 \pm 0.1) \times 10^{-6}$
$t_0$ (MJD)	50344.0	51068.906
$\chi^2/\text{dof}$	9.7/4	39.0/17

TABLE 4  
SPECTRAL FITTING RESULTS

Parameter	PCA model background	pulse minimum background
$N_{\text{H}}$	$(2.8 \pm 0.1) \times 10^{22} \text{ cm}^{-2}$	$(6.0 \pm 1.0) \times 10^{22} \text{ cm}^{-2}$
Power Law Photon Index	$1.17 \pm 0.01$	$1.01 \pm 0.08$
Power Law Normalization	$(1.93 \pm 0.05) \times 10^{-2}$	$(7 \pm 1) \times 10^{-3}$
$E_{\text{line}}$	$6.69 \pm 0.05 \text{ keV}$	...
$\sigma_{\text{line}}$	$0.4 \pm 0.1 \text{ keV}$	...
Gaussian Normalization	$(2.7 \pm 0.5) \times 10^{-4}$	...
$E_{\text{cutoff}}$	$13.3 \pm 0.2 \text{ keV}$	$11 \pm 1 \text{ keV}$
$E_{\text{fold}}$	$16.8 \pm 0.9 \text{ keV}$	$19 \pm 4 \text{ keV}$
Flux (2-10 keV)	$1.1 \times 10^{-10} \text{ ergs cm}^{-2} \text{ s}^{-1}$	$7.2 \times 10^{-11} \text{ ergs cm}^{-2} \text{ s}^{-1}$
$\chi^2/\text{dof}$	57.96/67	66.98/70

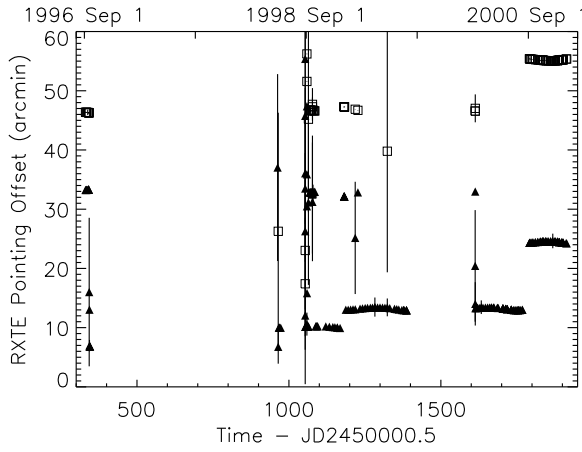


Fig. 1.— *RXTE* pointing offsets to XTE J1906+09 (filled triangles) and 4U 1907+097 (open squares) during SGR 1900+14 observations. Error bars indicate the standard deviation in the pointing offset. Scanning observations have the largest error bars. Gaps indicate times when each object was outside the *RXTE* field of view.

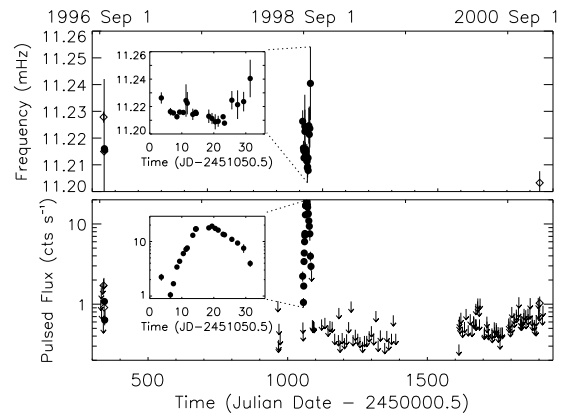


Fig. 2.— (Top): Frequency search results for XTE J1906+09. Barycentric corrections have been applied. Filled circles indicate 99.99% confidence detections and open diamonds indicate 99.9% confidence detections. The 99.9% confidence detection on MJD 51902 is likely due to contamination from 4U 1907+09. (Inset): Expanded view of pulse frequency detections during the 1998 outburst. (Bottom): Root mean squared 2-30 keV pulsed flux for XTE J1906+09. The count rate in all observations has been corrected for the offset pointing direction and scaled to the rate expected from 5 PCU if fewer PCU were active. Downward pointing arrows denote 99% confidence upper limits. (Inset): Expanded view of pulsed fluxes corresponding to frequency detections during the 1998 outburst.

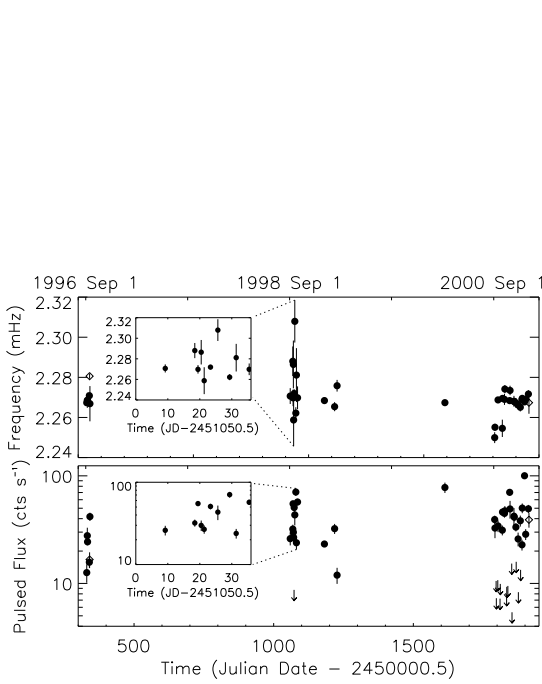


Fig. 3.— (Top): Frequency search results for 4U 1907+09. Barycentric corrections have been applied. Filled circles indicate 99.99% confidence detections and open diamonds indicate 99.9% confidence detections. (Inset): Expanded view of 4U 1907+09 pulse frequency detections during the 1998 outburst of XTE J1906+09. (Bottom): Root mean squared 2-30 keV pulsed flux for 4U 1907+09. The count rate in all observations has been corrected for the offset pointing direction and scaled to the rate expected from 5 PCU if fewer PCU were active. Downward pointing arrows denote 99% confidence upper limits. (Inset): Expanded view of 4U 1907+097 pulsed fluxes corresponding to 4U 1907+09 frequency detections during the 1998 outburst of XTE J1906+09.

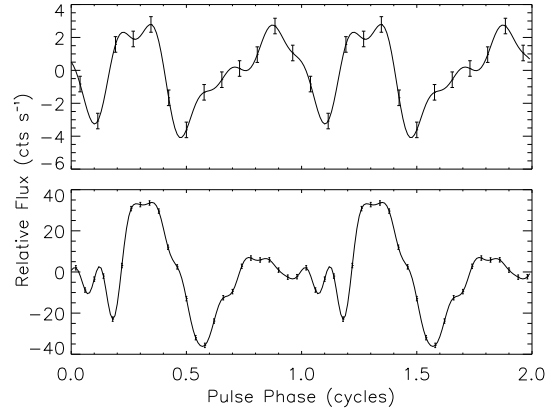


Fig. 4.— (Top): Mean subtracted pulse profile from MJD 50343 (1996 September 17) generated by fitting a Fourier expansion to 2-30 keV PCA event mode light curves. Only the first 6 harmonics were significant. (Bottom): Mean subtracted pulse profile from MJD 51072 (1998 September 16) generated by fitting a harmonic Fourier expansion to 2-30 keV PCA Good Xenon data light curves. Only the first 12 harmonics were significant.

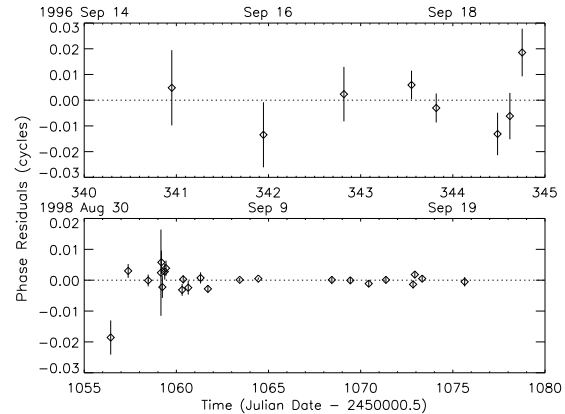


Fig. 5.— (Top): Phase residuals for a fit of a third order polynomial to connected pulse phase measurements from the 1996 outburst. (Bottom): Phase residuals for a fit to a fifth order polynomial to connected pulse phase measurements from the 1998 outburst.

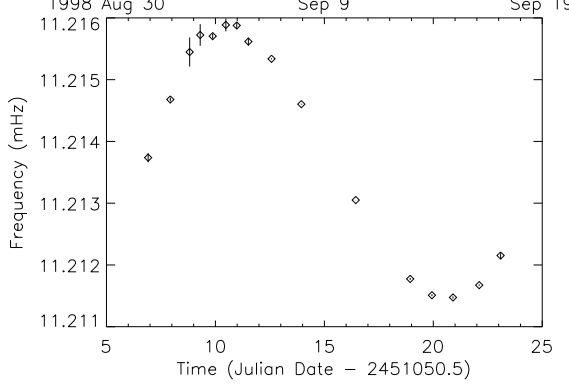


Fig. 6.— (Top): Barycentered pulse frequencies computed from connected phases for the 1998 outburst. A sinusoidal signature, likely due to orbital motion of the pulsar, is evident.

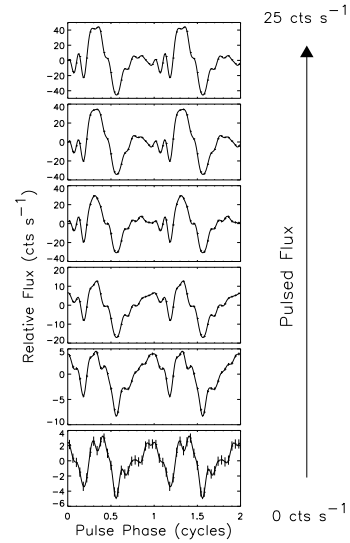


Fig. 8.— (Top 5 panels): Mean subtracted pulse profiles from the 1998 outburst averaged over time in 5 bands of 2-30 keV rms pulsed flux: 0-5, 5-10, 10-15, 15-20, 20-25 counts  $s^{-1}$ . The profiles were phase aligned using the polynomial model in Table 3. (Bottom panel): The pulsed profile from the brightest interval in the 1996 outburst (also shown in Figure 4) which had an rms pulsed flux of  $1.9 \pm 0.1$  counts  $s^{-1}$ . This profile has been aligned by eye with the 1998 pulse profiles.

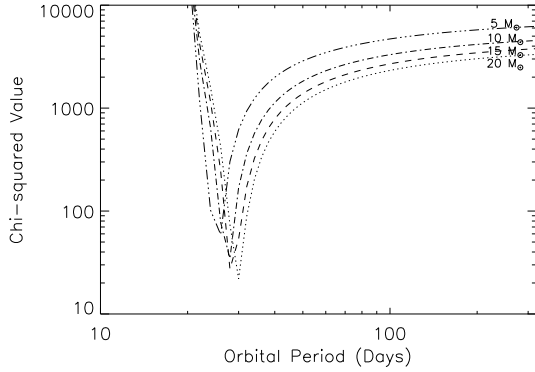


Fig. 7.—  $\chi^2$  versus orbital period for 4 mass functions  $f(M) = 5, 10, 15, 20 M_{\odot}$ . The orbital period and mass function were fixed for each grid point. The eccentricity, periapse angle, epoch of periastron passage, and the parameters of the quadratic phase model were allowed to vary in each fit to 23 phase points, giving us 17 degrees of freedom.

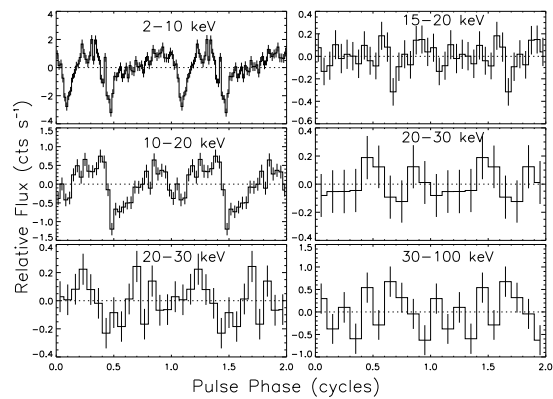


Fig. 9.— Mean subtracted pulse profiles from PCA (left) and HEXTE (right) data from 1996 September 17-18 epoch-folded using the phase model in Table 3. PCA profiles above 20 keV and all HEXTE profiles are consistent with a constant value.

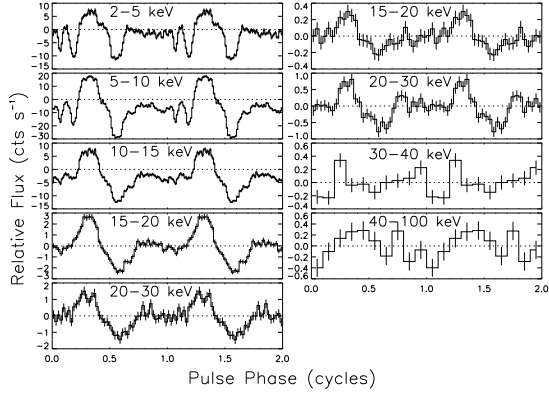


Fig. 10.— Mean subtracted pulse profiles from PCA (left) and HEXTE (right) data from 1998 September 8 epoch-folded using the phase model in Table 3.

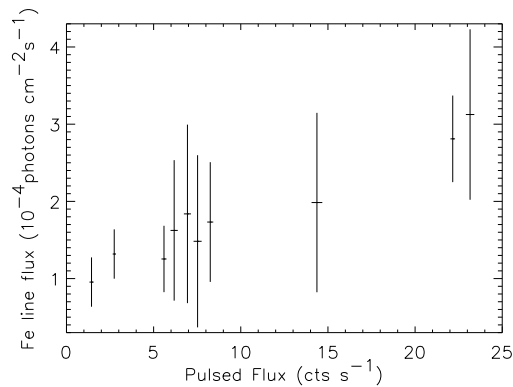


Fig. 11.— Integrated flux in the iron line at  $\sim 6.6$  keV versus 2-30 keV pulsed flux in  $\text{counts s}^{-1}$ . The iron line flux is correlated with the pulsed flux, with a correlation coefficient of 0.93 and a chance probability of  $10^{-4}$ , suggesting that the iron line is intrinsic to XTE J1906+09.

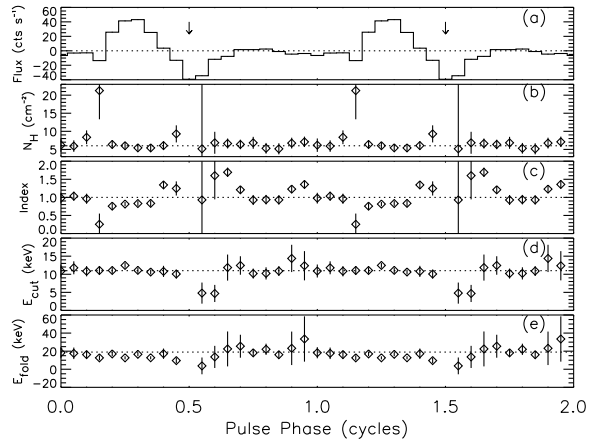


Fig. 12.— Phase dependence of spectral parameters of an absorbed power law with a high energy cutoff. (a) The mean subtracted 2-30 keV pulse profile divided into 20 equal bins. Each bin was fitted separately with XSPEC. The spectrum from pulse minimum, indicated using arrows on the plot, was used as the background spectrum for all spectral fits. (b) The absorption column density  $N_{\text{H}}$  in units of  $\text{cm}^{-2}$ . (c) The power law photon index. (d) The cutoff energy  $E_{\text{cut}}$  in keV. (e) The folding energy  $E_{\text{fold}}$  in keV.